Synthesis and characterization of montmorillonite/polyaniline composites and its usage to modify a commercial separator

Synthesis and characterization of montmorillonite/polyaniline composites and its usage to modify a commercial separator

M. L. Para[1], D. Versaci[1], J. Amici[1], M. F. Caballero[1], M. Cozzarin[2], C. Francia[1], S. Bodoardo[1], M. Gamba[3,4]

[1]Department of Applied Science and Technology, Institute of Chemical Engineering Politecnico di Torino. Corso Duca degli Abruzzi, 24, 10129, Torino, Italy.

[2]YPF Tecnología S.A., Av. del Petróleo Argentino S/N (entre 129 y 143), (B1923) Berisso, Buenos Aires, Argentina.

[3]Instituto de Investigaciones Fisicoquímicas Teóricas y Aplicadas, INIFTA, CONICET – UNLP,Diagonal 113 y 64 S/N La Plata, Bs. As., Argentina.

[4]Centro de Tecnología de Recursos Minerales y Cerámica, CETMIC, CIC-CONICET-UNLP, Camino Centenario y 506 (CP 1897) M.B. Gonnet., Argentina.

e-mail: maria.para@polito.it

Abstract

Composites of montmorillonite (MMT) and polyaniline (PANI) were synthetized through a facile and inexpensive method. Two samples with different MMT/PANI ratios were studied and deeply characterized by XRD, TG, zeta potential, FTIR and XPS measurements. On one hand, the sample with ratio MMT/PANI = 87/13 was an intercalated composite, were polyaniline resides between the inorganic layers of the clay at a regular distance. On the other hand, the sample with ratio MMT/PANI = 12/88 was an exfoliated composite, where the inorganic sheets are immersed in an amorphous polymeric matrix. FTIR and XRD results indicated that in both samples, the emeraldine form of polyaniline was obtained.

The composites were used to modify -by dr. blade technique- a commercial separator for lithium-ion batteries (LIBs) with the aim of increasing its wettability, ionic conductivity and electrochemical performance. The three-dimensional and multilayered network structure of the MMT/PANI composites led to an enhancement of the electrolyte uptake capacity (from 32% in bare Celgard to 137% and 168% for MMT/PANI_87/13 and MMT/PANI_12/88 modified separators, respectively, after 3 hours). The presence of the coating membrane also led to an increase of the ionic conductivity by one order of magnitude in the modified separators respect to the unmodified one.

These coated and non-coated separators were used to assemble full cells with $LiNi_{1.5}Mn_{0.5}O_4$ as cathode active material. The capacity fade after 200 cycles was 20% lower in the cell with MMT/PANI_12/88 membrane in comparison with the bare separator.

The enhancement of the electrochemical performance of the cells with the coated separator suggests that is a promising strategy to be used in LIBs.

Keywords

Montmorillonite - polyaniline- clay/polymer composite - modified separator - lithium ion battery

1. Introduction

Organic electroactive materials are being widely studied in energy storage systems, since their electrochemical and physicochemical properties allow the design of a wide variety of structures that adapt to current needs [1]. Organic polymers have become especially relevant in various fields because of their unique properties, such as mechanical flexibility, chemical resistance, excellent processability and lightness [2]. Among them, the metal-like electron conduction of inherently conducting polymers makes them extensively used in different devices as supercapacitors, lithium ion batteries (LIB) and lithium sulphur batteries (LSB). For example, separators composed by p-polyphenyl (PPP)/polyaniline (PANI), poly(3-butylthiophene) (P3BT), poly(3-decylthiophene) (P3DT) or polytriphenylamine (PTPAn), have been used as a potential-sensitive switch to maintain the charge voltage in LIBs [2]. In addition, taking into account that this kind of polymers are both electronically and ionically conductive, their usage as functional interlayer in LSB is beneficial to reduce the resistance, enhance the rate capability of the cell and prevent the *shuttle effect* during charge/discharge cycles. For example, it is reported that proton-doped polypyrrole (PPy), poly(3,4-ethylenedioxythiophene) (PEDOT), polythiophene (PTh) and polyaniline (PANI) develop H-bonds that act as bridges linking the polymers to the polysulfides anions [3,4]. Over other conducting polymers, PANI has greater advantages due to its comparatively much simpler and cheaper synthesis, high thermal and environmental stability and unique doping/dedoping mechanism. There are typically three oxidation states of PANI: leucoemeraldine base, emeraldine base (EB) and pernigraniline base which are the fully reduced, half-oxidized and fully oxidized species, respectively [5]. The half-oxidized EB possesses alternating quinoid and benzenoid rings. When it is 50% doped, the emeraldine salt (ES) is formed, presenting a polaron structure, responsible for the highest conductivity of PANI species (about 10^3–10^4 S cm^{-1}) [6].

The combination of PANI with well-ordered materials to form composites is a way to avoid the problems related to its insolubility in common solvents and its poor crystalline nature that make it difficult to handle ([7] and references therein). Chang et al., 2015 [8] reported a PANI nanofiber/multiwall carbon nanotube (PANINF/MWCNT) mixture used as coating onto a commercial polypropylene in LSB. The PANINF/MWCNT coating provided an electron transfer channel, and efficiently inhibited the migration of soluble polysulfides as well as it retained a high reversible capacity of 709 $mAhg^{-1}$ after 100 cycles at 0.2 C [3].

Montmorillonite (MMT) is an abundant and low-cost phyllosilicate. Its layered structure, high specific surface area and cation exchange capacity allow concentrating a huge amount of positive aniline monomers in its galleries. By means of an in-situ chemical oxidation it is possible to grow PANI in the interlamellar sites of MMT to obtain oriented polymer chains. The composites MMT/PANI formed by this strategy have different behaviour from the starting materials, such as better mechanical and thermal properties [9]. These properties could be managed by changing the ratio MMT:PANI and the doped state of PANI, and this versatility has attracted attention in the last decades [7]. According to this, the composite MMT/PANI has been applied in corrosion protection [10], in metal adsorption from aqueous solution [11], in the detection of trace heavy metals [7]. Also, electrically conductive and optically transparent MMT/PANI nanocomposite thin films were achieved [12]. However, to the best of our knowledge, MMT/PANI composites were not studied as functional interlayer or separator modifier in LIB [3].

Among the commercial separators for LIB and LSB there are polyethylene (PE) and/or polypropylene (PP) stretch membranes [13]. Different techniques have been developed to reduce their low wettability with liquid electrolytes and weak thermal and mechanical stabilities, such as polymers surface grafting modification, ceramic coatings, or their replacement with nonwoven membranes or polymer electrolytes [13–15]. For example, Zhang et al., 2015 [13] prepared a separator from cellulose nanofibers (CNF) that exhibited higher porosity (70%) than that of commercial PP separator (40%) and was wetted in a few seconds. In terms of cyclability, cells assembled with CNF and PP separators retained 91.7% and 87.8% of the capacity after the 100th cycle, respectively. Another methodology was reported by Shi et al., 2017 [14]: they showed that a ceramic coating separator prepared with PE, Al_2O_3 and polydopamine (PDA) through a simple chemical deposition method exhibited improved wettability and high ionic conductance while the cells with modified separator showed similar electrochemical behaviour to the bare PE separator. -Finally, Yang et al., 2017 [16], proved that coating a PE separator with an organic-MMT/PPy composite was beneficial to improve the absorbent ability of organic electrolyte and the migration of Li^+, to enhance thermal stability, to inhibit the disproportionation of Mn^{3+} in $LiNi_{1/3}Co_{1/3}Mn_{1/3}O_2$ cathode materials and to decrease the internal resistance of the cell at high temperature.

In this study, aniline was polymerized in presence of inorganic layers of MMT. MMT/PANI composites with different MMT:PANI ratios were deeply characterized. A suspension formed by the composite, poly(vinylidene fluoride) (PVDF) and N-methyl

pyrrolidone (NMP) was coated onto the surface of a commercial (PP/PE/PP) separator, Celgard 2325. The electrochemical performance of the MMT/PANI-coated separator was explored as a strategy to increase cycling performance of high voltage cathode materials ($LiNi_{1.5}Mn_{0.5}O_4$), as a possible application to the composites synthesized.

2. Material and methods

2.1 Materials

A Patagonian (Rio Negro province, Argentine) montmorillonite sample, provided by Castiglioni Pes and Cia., was used as received and labelled MMT. The sample was characterized in previous work [17,18]. The isoelectric point (IEP) = 2.7, specific surface area (SSA) = 34.0 m^2/g, total specific surface area (TSSA) = 621 m^2/g. XRD and chemical analysis indicated that the sample contained Na-montmorillonite with quartz and feldspars as minor phases. The structural formula was $Si_{3.81}Al_{0.19}(Al_{1.40}Fe^{3+}_{0.27}Mg_{0.32})O_{10}(OH)_2(Na^+_{0.37}Ca^{2+}_{0.06}K^+_{0.02})$. The cationic exchange capacity (CEC) was 87.3 ± 0.8 mmol/g clay.

The reagents, $(NH_4)_2S_2O_8$ (PSA), H_2SO_4, aniline, N-Methyl-2-Pyrrolidone (NMP) and polyvinylidene fluoride (PVDF) were analytical grade and used as received from SIGMA-ALDRICH®. The cathode and anode were provided by Lithops/FAAM and used as received. The cathode contained 90% LNMO (from NEI Corporation), 5% C-65 and 5% PVDF. The active material mass loading was around 7 mg cm^{-2}. Meanwhile, the anode consisted in 94% advanced graphite, 1.5% C-45, 2.5% carboxy methyl cellulose (CMC) and 2% styrene-butadiene rubber (SBR). The separator was a polypropylene Separator Monolayer PP Celgard 2325 (thickness: 25 µm; porosity: 55%, pore size: 0.064 µm).

2.2 Preparation of MMT/PANI composites and MMT/PANI modified separator.

MMT/PANI composites were prepared by chemical oxidation following a method adapted from [12] and [19]. A suspension of MMT was prepared and kept 0.5 hours under sonication to favour the delamination. A monomer solution ([aniline] = 0.2 M in [H_2SO_4] = 0.5 M) was slowly added to the montmorillonite suspension with constant stirring. The obtained suspension was sonicated for 0.5 h and then stirred for another 4 h. The oxidant agent (PSA) [$(NH_4)_2S_2O_8$] = 1M was added drop by drop, until a molar ratio aniline:PSA = 1:1 was achieved. The colour of the samples turned to dark green (characteristic of

emeraldine salt state of polyaniline). The reaction was kept stirring overnight. The obtained precipitates were filtered, washed with distilled water several times until neutral pH was achieved. The samples were dried overnight at 60 °C. A pure PANI sample was prepared as a blank following the same procedure but without the addition of MMT.

Two composites with different monomer/clay ratio were prepared (see Table 1). The samples were labelled according to the MMT/PANI mass ratio determined by thermogravimetric (TG) measurements. With the objective of obtaining two distinct morphologies and properties, two extreme ratios were selected and evaluated. Additionally, a 50:50 composite was prepared, with no improvement of the electrochemical performance (Figure SI 1). For this reason, this sample was not deeply characterized.

The commercial Celgard 2325 separator film was modified by dr. blade technique. The slurries were obtained by mixing PVDF and the different composites in NMP using ball milling, with a ratio composite:PVDF = 80:20. The obtained coated separators were dried at RT and then cut into discs of 20 mm diameter.

Table 1. Amounts of monomer and clay used in the synthesis of the composites and MMT:PANI expected and obtained ratios (bulk (TG) and superficial (XPS)).

Sample	Clay mass (g)	Aniline mass	MMT:PANI (expected)* (w/w)	MMT:PANI TG (w/w)[#]	Si:N XPS[#]
MMT/PANI_12/88	0.1	1.95	4.1:95.9	11.5:88.5	7.8/92.2
MMT/PANI_87/13	1	0.195	86.7:13.3	86.5:13.5	88.9/11.1

*considering a polymerization yield = 100%

[#]this is discussed in results section

2.3 Characterization methods and electrochemical tests

Thermogravimetric analyses (TG) were carried out using a NETZSCH TG 209F3 with alumina as a reference. Samples of 20 mg were placed in Al_2O_3 crucibles and heated from 25 to 800 ºC at a rate of 10 ºC/min in air atmosphere. The differential thermogravimetric (DTG) curves were directly derived from the corresponding TG curves.

Powder X-ray diffraction technique (XRD) was performed for each sample as well as for bare MMT to verify the structural configuration. XRD patterns were collected on random powder samples from 5 to 40º (2θ) with a counting time of 10 s/step and 0.026º (2θ) step size, using a PANalytical X'Pert (Cu Ka radiation, λ = 0.154187 nm) diffractometer

with a 2D solid state detector (PIXcel). The basal spacing was calculated from the diffraction d(001) peak of MMT using Bragg's equation; $n\lambda = 2d \sin\theta$.

Zeta potential vs pH curves were constructed measuring electrokinetic potentials with a Brookhaven 90Plus/Bi-MAS equipment (electrophoretic mobility function). The electrophoretic mobility was converted into a zeta potential value using the Smoluchowski equation. For each determination, 10 mg of sample was dispersed in 10 mL of 1.10^{-3} M KCl solution (used as inert electrolyte), and the pH was adjusted adding drop by drop different concentrations of HCl or KOH followed by magnetic stirring until the equilibrium was attained (10 min).

XPS analyses were performed on a computer equipped with a Multitechnic Specs with dual X-ray source of Mg/Al and XR50 model Phoibos 150 hemispherical analyser, in transmission mode fixed analyser (FAT). The spectra were obtained using a not monochromatic Al Kα radiation (h = 1486.6 eV) operated at 100 W and 10 kV. The pass energy for the survey scan was 30 eV. The survey scan range was 1200–10 eV and dwell time 100 ms. During measurements, the pressure was 2.10^{-6} Pa. Samples were supported on a double sided Cu tape and then subjected to ultra-high vacuum evacuation for 12 h prior to the XPS analysis. To minimize the effects of surface charge the experiments were carried out with Flood Gun 1 eV ignition energy. The C-(C, H) component of the C 1s peak of carbon has been fixed to 285 eV to set the binding energy scale. Molar fractions were calculated using peak areas normalized on the basis of acquisition parameters after Shirley background subtraction. Sensitivity factors, Mean Free Path, and transmission factors were provided by the manufacturer. High resolution spectrum of Si 2p and N 1s were collected to determine their relative areas.

Fourier Transform Infrared Spectroscopy (FTIR) was measured with a NicoletTM iS50 FTIR spectrometer (Thermo ScientificTM) equipped with ATR tool. 32 scans were collected with a resolution of 4 cm^{-1} from 4000 to 400 cm^{-1}.

The morphology of modified separators was examined using field-emission scanning electron microscopy (FESEM, ZEISS Supra 40).

Electrolyte contact angles measurements were performed at room temperature using a Drop Shape Analyzer DSA 100 Krüss (the drop volume was 10 µL).

The capacity of the separators to uptake (φ) and to retain (ρ) the liquid electrolyte was calculated using the following equations:

$$\varphi = \frac{w1 - w0}{w0}\ x\ 100\% \quad (1)$$

$$\rho = \frac{w1 - w0}{w1}\ x\ 100\% \quad (2)$$

where w0 is the weight of dry separator and w1 is the separator weight after soaking in electrolyte and removing excess electrolyte on the surface. Discs of the separators with and without coating where soaked into the electrolyte and both the electrolyte uptake and the electrolyte retention where measured after 3, 24 and 144 hours for each sample

Ionic and electronic conductivities were calculated from resistance values obtained by impedance spectroscopy. The measurements were performed using two stainless steel blocking electrodes in the frequency range from 1 Hz to 1.10^5 Hz with amplitude of 10 mV at open circuit potential. Two methods were followed: (i) To determine ionic conductivities, the coated and not coated separators were wetted with electrolyte and then impedance measurements were performed at different temperatures, from 25 °C to 65 °C. The electrolyte used was a commercial 1M $LiPF_6$ in ethylene carbonate (EC) and dimethyl carbonate (DMC) (1:1 v/v) + 1% vinyl carbonate (VC). (ii) To determine electronic conductivities of the composites, the previously described slurries were blade casted on aluminium foils. The measurements were carried out for bare aluminium as well as coated aluminium foils. In both cases, conductivities were calculated from the resistance values according to Equation (3):

$$\sigma = \frac{L}{R_b\ x\ A} \quad (3)$$

where R_b, A and L take different values depending on the method. To determine ionic conductivity of the separators (method I), R_b, A and L are the separator bulk resistance, area and thickness, respectively [16]. To determine electronic conductivity of the composites (method II), R_b is the difference between the resistance values obtained for the coated aluminium disc and that obtained for the bare aluminium foil [20]; A is the area of the disc and L is the coating thickness.

Electrochemical properties were studied by preparing 2032 coin cells assembled in an Argon filled glove box with water and oxygen levels maintained below 1 ppm. All tests were performed using a multichannel galvanostat BR-2000 (Arbin Instrument) at room temperature. Full cells were assembled using LMNO as cathode and graphite as anode. In each case, after 10 cycles at C/10, 200 galvanostatic charge/discharge cycles were performed at C/5 between 3.5 and 4.9 V *vs*. Li^+/Li. C rates are referred to LNMO mass.

3. Results & Discussion

3.1 Characterization of obtained composites

The MMT:PANI bulk ratios as well as the thermal stabilities of the composites were studied by TG measurements. Figure 1 presents the TG and DTG curves of MMT, pure PANI and the obtained MMT/PANI composites.

As expected, MMT shows two mass loss stages: the first between 25 and 200 °C (8.7% mass loss) and the second between 400 and 800 °C (4.1% mass loss). The first jump in the TG curve leads to two DTG peaks in MMT: the first and more intense peak at 88 °C corresponds to the desorption of water molecules weakly bonded to the outer surface or pores of the clay. The second, less intense peak at 125 °C corresponds to water molecules coordinated to the naturally occurring exchangeable inorganic cations located between the negative siloxane layers of MMT. The second jump in the TG curve is associated with a DTG peak at 660 °C and attributed to the dehydroxylation of the octahedral structure of MMT. In the whole 200-800 °C interval, the mass loss is 4.5%.

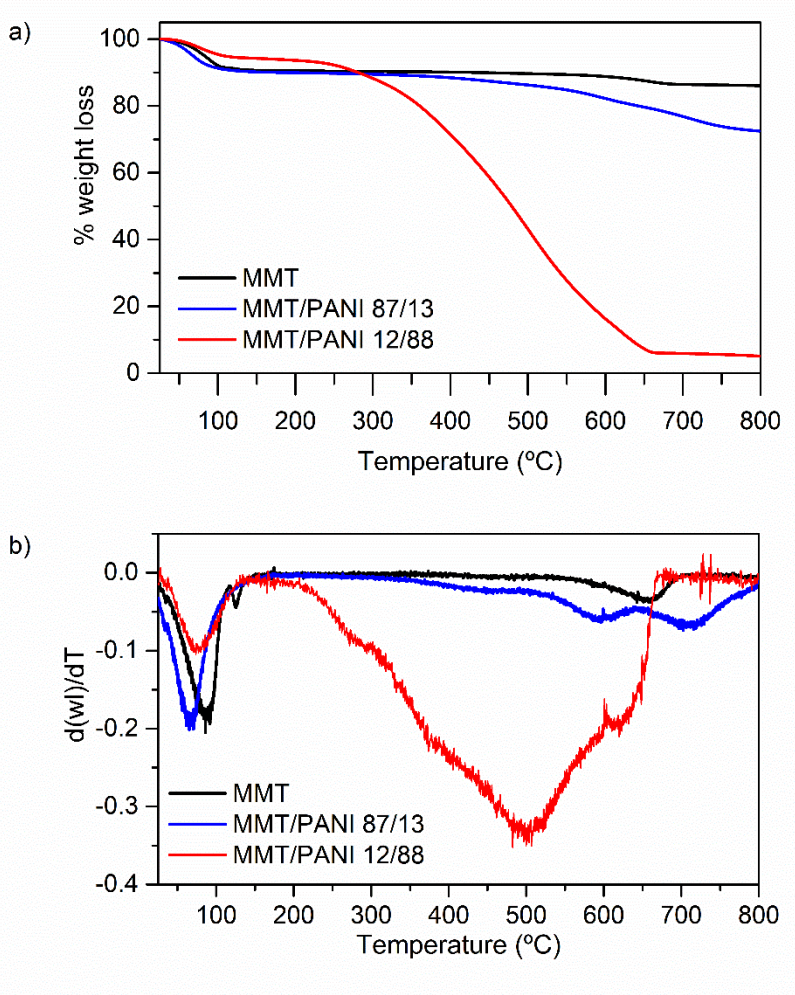

Figure 1. (a) TG and (b) DTG curves of raw montmorillonite and MMT/PANI composites.

The TG of pure PANI (Figure SI 2) was determined with the aim of understanding the thermal behaviour of the composites. It also shows two mass loss stages. The jump below 150 °C is due to the release of physically adsorbed water (6.4%) while above 220 °C, PANI starts its thermal decomposition and is completely decomposed at 680 °C (91.5% mass loss). The last TG jump leads to a wide DTG peak centred at 504 °C. It is assumed that the superimposition of combustion, vaporization, fusion sublimation and/or decomposition of PANI backbone chains occurs in this temperature range [21].

The TG and DTG curves of MMT/PANI composites (Figure 1) show two jumps associated with the above-mentioned processes. In the composites the peaks related to the first step of water release are shifted to lower temperatures, from 88 °C in MMT to 77 °C and 66 °C in MMT/PANI_87/13 and MMT/PANI_12/88, respectively, suggesting that

the hydrophilicity of the MMT surface due to the hydrated inorganic cations has decreased. Furthermore, the second small peak observed in MMT (at 125 °C) is absent in both composites, confirming the total exchange of the inorganic cations by anilinium during the synthesis.

The region between 200-800 °C was different among the composites. On one hand, for MMT/PANI_87/13, a total mass loss of 17.4 % and four DTG peaks (at 452 °C (weak), 593 °C, 608 °C and 711 °C) are registered (Figure 1). However, the main thermal decomposition (13.8% mass loss) occurs from 500 to 800 °C. The DTG peaks at 593 °C, 608 °C and 711 °C are assigned to the decomposition of PANI chains, the dehydroxylation of MMT and the final combustion of high thermal stable charcoal, respectively [22]. This increase in the thermal stability of PANI chains in the composite compared to pure PANI is justified by the barrier effect of the clay layers. During decomposition, the clay layers dispersed in the polymer matrix slow down the distribution of gaseous oxygen and the resulting products, so that the degradation is prolonged and the thermal behaviour improves [23]. Besides, the shift of the DTG peak associated with the MMT dehydroxylation to lower temperatures evidences the interaction between the polymer and the clay layers. Such an effect is usually observed in organically modified clays and attributed to the penetration of the charged heads of organic cations into the siloxane layer [24]. These results are in agreement with Lee & Char, 2002 [25] who proposed that to enhance the thermal stability of the polymer/clay composite is necessary to achieve an intercalated nanostructure.

On the other hand, in the range of 200-800 °C, MMT/PANI_12/88 exhibits a behaviour quite similar to pure PANI: the composite starts to decompose above 200 °C and finishes at 690 °C with a mass loss of 88.7% resulting in the wide DTG peak centred at 506 °C (Figure 1 b). In this sample, the immobilization of PANI chains on the MMT surface cannot be proved, probably due to the excess of PANI in the PANI/MMT composite [12]. Lee & Char, 2002 [25] showed that with PANI contents above 12.3 wt.%, the excess of PANI chains resides mainly outside the siloxane layers of MMT as free PANI chains and its thermal decomposition can occur in both confined and free states at the same time. However, the contribution to the thermal decomposition of free PANI chains may be more significant because these chains are more exposed to heating than PANI chains intercalated between the siloxane layers.

Based on the above discussion, the expected MMT:PANI ratios (w/w) (Table 1) were calculated following the stoichiometry proposed in Scheme 1. For MMT/PANI_87/13,

the amount of starting monomer corresponded to 95% CEC of the clay. Therefore, it is expected that in the initial suspension, each positively charged anilinium ion was attached to a negative permanent charge site of MMT. If the reaction proceeds with 100% yield, after the addition of oxidizing agent (PSA) to the suspension, all the anilinium polymerize between the clay sheets. As a product, an intercalated nanocomposite where the emeraldine positive charges are neutralized by the negative layers of MMT, is obtained (Scheme 1, A). Conversely, for MMT/PANI_12/88, the initial amount of anilinium highly exceeded the 100% CEC value. Thus, most of the anilinium ions form a salt with HSO_4^- as a counter ion, which must be taken into account in the stoichiometry of the reaction, both in the starting reagent and in the product (Scheme 1, B). The addition of PSA leads to "free" emeraldine salt chains.

The actual MMT:PANI ratio (w/w) (Table 1) in each composite was determined by subtracting the percentage associated with the dehydroxylation of MMT from the mass lost in the interval 200-800 °C taking into account the expected MMT:PANI ratio. As shown in Table 1, for MMT/PANI_87/13 the expected MMT:PANI ratio and that obtained from TG are exactly the same, which indicates that the model proposed is correct. Instead, MMT/PANI_12/88 shows a higher MMT:PANI ratio than the expected, suggesting that anilinium ions were partially polymerized (yield lower than 100%) and/or some oligomers with low molar mass was lost in the washing water [26].

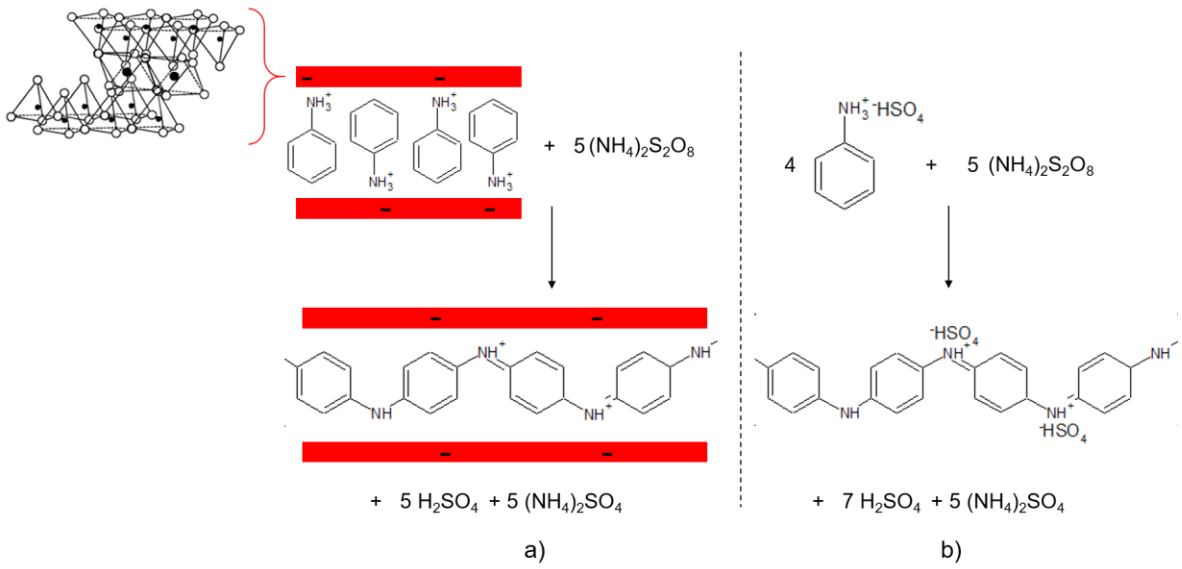

Scheme 1. a) The polymerization of anilinium in the interlamellar space of MMT form an intercalated nanocomposite where the emeraldine positive charges are balanced with the negative charges of MMT. b) In presence of very low content of MMT the polymerization of anilinium.$^-HSO_4$ bring as product "free" emeraldine salt chains.

The XRD patterns of MMT and MMT/PANI composites are shown in Figure 2. The characteristic 001 peak of MMT is at $2\theta = 8.6°$, corresponding to a basal spacing of 10.3 Å. The de-hydrated MMT has an interlayer distance of 9.7 Å [27], so the enlargement of the basal space is attributed to the hydration spheres of naturally occurring inorganic cations in the interlamellar space.

The XRD patterns of the MMT/PANI composites are very different from each other (Figure 2). On one hand, the MMT/PANI_87/13 sample has the highest content of clay and shows a basal spacing of 14.2 Å (001 peak at $2\theta = 6.2°$)). This increase in the basal spacing -compared to bare MMT- is related to the exchange of the inorganic cations by anilinium ions followed by the polymerization of PANI in the MMT galleries. Furthermore, the peak is sharper and more intense in MMT/PANI_87/13 sample than in bare MMT, indicating a greater homogeneity in the interlaminar distance in the former than in the latter. Such results, in addition to TG analyses and clay/polymer ratio, confirm that this sample is an intercalated composite system, where polymer chains reside between the tactoids layers at a regular distance [19].

On the other hand, MMT/PANI_12/88 shows a low crystalline pattern. The 001 peak is at $2\theta = 6.5°$ (basal spacing = 13.6 Å), has very low intensity and is very wide, and new peaks in the interval 19.5-25.6 °(2θ) characteristic of PANI appeared. These peaks are assigned to the emeraldine form of PANI and are ascribed to the parallel and perpendicular periodicity to the PANI chain direction, respectively [20,28]. This observation agrees with both the clay/polymer ratio and TG results, where it was not possible to demonstrate the interaction of PANI with siloxane clay sheets, and on the contrary, the presence of "free" chains was postulated.

For both composites, the interlayer thicknesses are determined by the difference between the basal space of the samples and that of the dehydrated clay (9.7 Å). The calculated interlayer thicknesses are 3.9 Å and 4.5 Å for MMT/PANI_12/88 and MMT/PANI_87/13, respectively. These results are related to a single chain of PANI in the galleries of the clay [26,29]. It is relevant that a higher polymer content in MMT/PANI_12/88 did not lead to an increase in the basal spacing (on the contrary, it is slightly lower), as previously reported [26]. If MMT/PANI_87/13 was postulated as an intercalated system with most of the polymer between the clay sheets, MMT/PANI_12/88 sample is considered as an exfoliated composite [19], with high stacking disorder of the clay layers dispersed through the polymeric matrix. However, for the exact description of

the morphology of the composites, XRD analysis should be coupled with SEM techniques, as further discussed below.

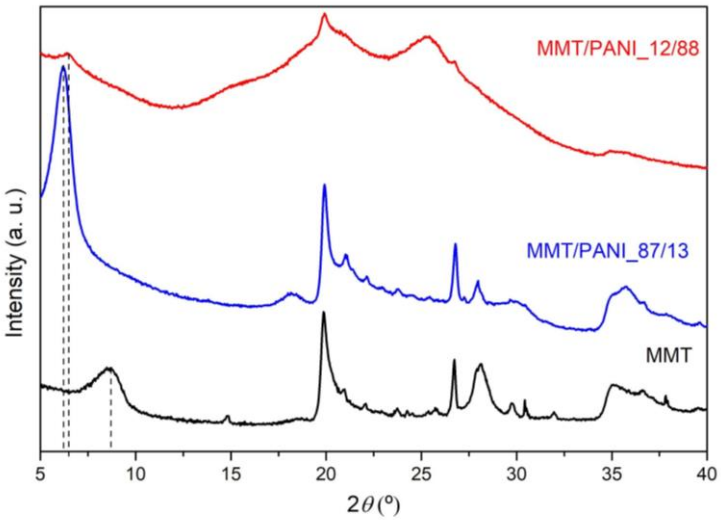

Figure 2. XRD patterns obtained for MMT and MMT/PANI composites.

Zeta potential measurements reflect changes in the electrical surface charge on the external surface of the samples [30]. Figure 3 shows zeta potential vs pH curves for MMT and MMT/PANI composites. MMT presents two types of surface charges: permanent charged sites (negative interlamellar sites) and pH-dependent charged sites (edges). Since the latter represent only 1% of the total external surface, the zeta potential of MMT presents negative values for the entire pH interval (about -37 mV). On one hand, the zeta potential of MMT/PANI_87/13 in the whole interval of pH is almost the same as MMT, indicating that in the composite the polymer is preferentially located in the interlaminar space and not on the external surface, which is in agreement with XRD and TG analyses. On the other hand, the sample with a higher content of polymer, MMT/PANI_12/88, showed an isoelectric point (pH at the point of zero charge, pH_{pzc}) within 6.8 and 7.5. Although a direct correlation between pH_{pzc} and pK_a is not possible (since polyaniline emeraldine salt is a polyelectrolyte with a wide dispersion of pK_a values [31]), the positive zeta potential values can be related to an increase in the doping degree of PANI-ES, i.e. imine groups that are further protonated [32]. This behaviour is in agreement with Scheme 1 and with the proposed model where MMT sheets are immersed in the PANI-ES matrix.

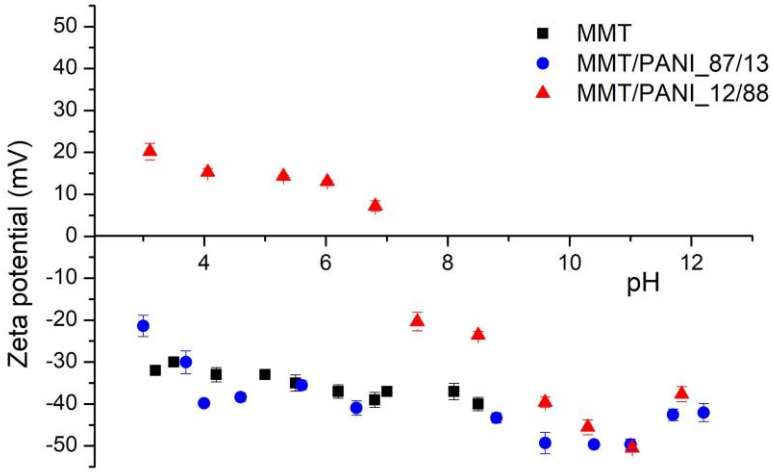

Figure 3. Zeta potential measures of indicated samples.

The chemical composition of the samples was determined by XPS analysis. It is worth mentioning that the XPS technique is sensitive to the surface (~5–10 nm depth) and therefore the results describe well the external surface of the samples but may not refer to the actual bulk composition. The XPS survey scan confirm the presence of Na^+ in MMT (~498 eV, yellow dot in Figure 4, A), whereas its absence in MMT/PANI composites confirm its exchange by anilinium ions during their synthesis (in agreement with XRD and TG results). MMT also shows the bands assigned to Si 2p (~103 eV) and O 1s (~532 eV) constituents of the silicate framework, C 1s (285-289 eV) coming from an adventitious origin, and in smaller quantities Al 2p (~75 eV) and Mg (~306 eV, pink dot in Figure 4) [33]. The XPS spectra of the composites show a new signal at ~400 eV assigned to N 1s and an increase in the intensity of the C 1s peak associated with the presence of PANI in the samples. Particularly, MMT/PANI_12/88 presents a small amount of S (coming from the doping agent HSO_4^-, Scheme 1) and the typical MMT signals (Si, Mg, Al) have very low intensity or disappeared.

Since N atoms are exclusively from PANI and Si atoms entirely come from siloxane layers of MMT, the ratio Si:N reflects the surface ratio MMT/PANI [19]. The relative percentages of Si:N obtained (Table 1) are in agreement with the expected MMT/PANI ratios calculated based on Scheme 1. In addition, the Si:N ratio in the sample MMT/PANI_87/13 is slightly higher than the MMT/PANI ratio determined from TG (which represents the actual MMT/PANI in the bulk). This indicates that for this composite, the highest proportion of polymer is located in the interlaminar zone of the clay. An opposite

behaviour is found for MMT/PANI_12/88, where the Si:N ratio on the outer surface is lower than that obtained from TG. This indicates that the clay sheets are immersed in the polymer matrix and only a small amount remains exposed to the surface. These results are in agreement with zeta potential analyses and reinforce the models and reaction scheme previously proposed.

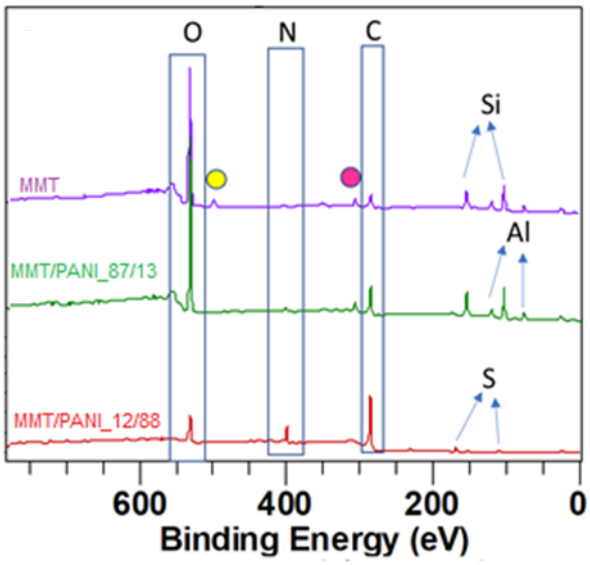

Figure 4. XPS survey spectra of indicated samples.

The FTIR spectrum of MMT and MMT/PANI composites are shown in Figure 5. The MMT spectrum shows the characteristic absorption bands related to the stretching and bending vibrations of its structural groups. The main peaks are assigned to υSiO (992 cm^{-1}), δAlAlOH (914 cm^{-1}) and δAlMgOH (880 cm^{-1}) while the band at 1636 cm^{-1} is attributed to OH deformation of water bonded to inorganic cations in the interlayer space. For both composites, the last peak is absent, confirming the ion exchange of the natural inorganic cations by anilinium during the synthesis of PANI.

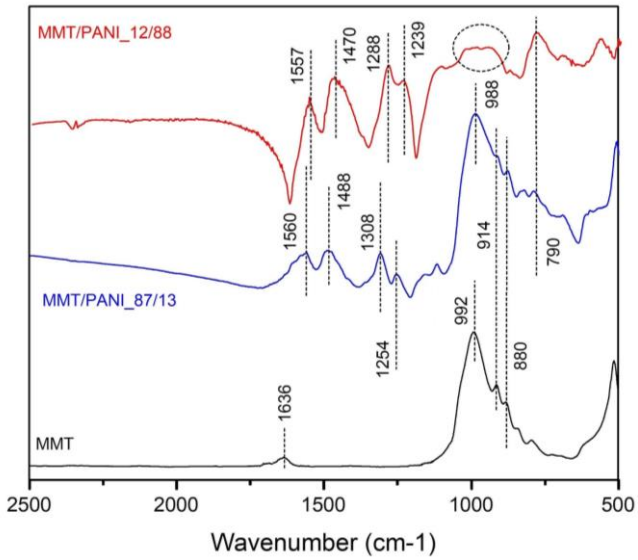

Figure 5. FTIR spectrum of indicated samples.

The FTIR spectrum of MMT/PANI_87/13 is the superposition of the polymer spectrum with that of MMT since the peaks of MMT are clearly identified while some new peaks characteristic of PANI are also found. Instead, in the spectrum of MMT/PANI_12/88 it is not possible to identify peaks associated with the clay, due to the very low content in the sample. Furthermore, MMT/PANI_12/88 shows the typical PANI-ES broad absorption band at wavenumbers higher than 2000 cm^{-1}. The so-called 'Fano effect' results as a consequence of overlapping of two types of photon absorption: a discrete absorption (centred in a certain frequency) and a continuous absorption (due to the continuous of electronic states of the polaron structure) [34,35]. The peaks at 1557 and 1560 cm^{-1} are assigned to the C=C stretching mode of the quinoid diimine structure (υC=C quinoid) while those at 1470 and 1488 cm^{-1} are due to the C=C stretching mode of the benzenoid structure (υC=C benzenoid) [26,36]. The bands occurring at 1288 and 1239 cm^{-1} in MMT/PANI_12/88 are attributed to the stretching vibration of C-N^{+} benzenoid and quinoid (υC-N+), respectively. These bands are generally related to the delocalization of the π-electron induced in the polymer by protonation [9,20] and confirm the existence of PANI as emeraldine salt. In MMT/PANI_87/13 sample, these bands are shifted to 1308 and 1254 cm^{-1} respectively, indicating the interaction between the N^{+} groups and the negative surface of the clay [37], in agreement with TG analyses. Finally, the broad band between 890 and 1074 cm^{-1} in MMT/PANI_12/88 (showed as a circle in figure 5) indicates the presence of some sulphate groups [9]. As was previously discussed, the positive charges

of the polymer backbone are balanced by the presence of HSO_4^- (dopant) in the vicinity of the polymer chains (Scheme 1).

3.2 Characterization of the (non)-coated separators

Figure 6 shows the SEM images of the coating layers on the modified Celgard 2335. Both samples present a three-dimensional and multilayered network structure (cross section images are shown in Figure SI 3, where the thickness of the coating is specified). On one hand, MMT/PANI_12/88 (Fig. 6 a-b) exposes a high percentage of PANI agglomerates on the surface. Furthermore, it is not possible to distinguish MMT flakes, because the amount of polymer is enough to cover them all. This morphology is in agreement with the proposed characterization and confirms that MMT/PANI_12/88 sample is an exfoliated composite with a high dispersion of clay layers through the polymeric matrix [19].

On the other hand, the SEM images of MMT/PANI_87/13 coating layer (Fig. 6 c-d) show clearly the flakes corresponding to the strati of MMT, since in this composite the PANI chains are located mostly in the interlayer space of MMT (in accordance with XRD, XPS, TG and zeta potential analyses). This sample is an intercalated composite system, where polymer chains reside between the tactoids layers at a regular distance.

SEM images of MMT/PANI_12/88 show granules of PANI whereas MMT flakes cannot be seen indicating that PANI chains are completely covering the MMT surface. This morphology reinforces XRD and zeta potential results and points out that MMT is immersed in the PANI matrix. In a similar sense, for MMT/PANI_87/13, MMT strati are not visible. This kind of intercalated structures was reported in previous works [38,39].

Figs. 6 b-d show polymer filaments of the PVDF binder, which maintains the integrity of the slurries and keep them attached to the Celgard separator. Both coated separators present a high specific surface area that could contribute to a higher electrolyte uptake. This would be beneficial to improve the migration of Li^+ and to increase the ionic conductivity, as further discussed below.

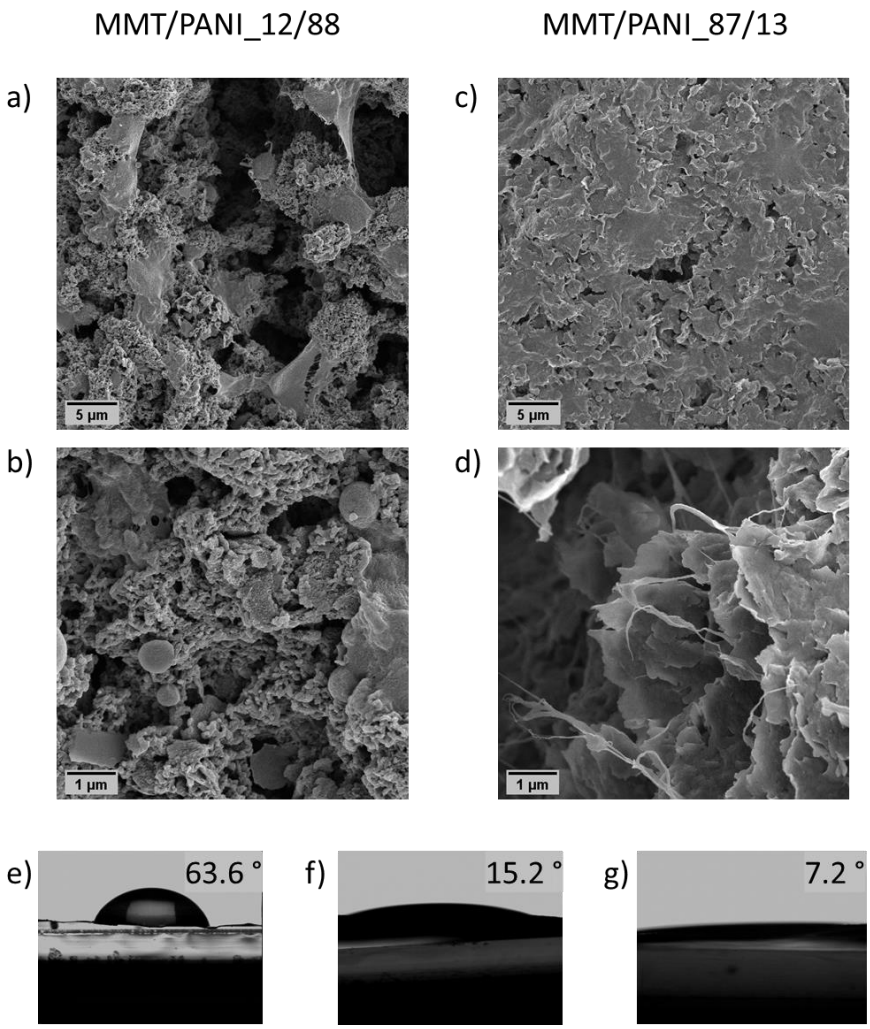

Figure 6. SEM images of Celgard 2325 modified with a layer of MMT/PANI_12/88 (a-b), and MMT/PANI_87/12 (c-d), at different magnifications; contact angles of the electrolyte on bare Celgard 2325 (e) and Celgard modified with a layer of MMT/PANI_87/13 (f) and MMT/PANI_12/88 (g).

In order to investigate the effect of the MMT/PANI composites layers on the wettability of the separators, contact angle measurements with electrolyte droplets were conducted. As shown in Fig. 6 (e-g), the static electrolyte contact angles of the separators decrease from 63.6° for the bare separator to 15.2° and 7.2° for the MMT/PANI_87/13 and MMT/PANI_12/88 modified separators, respectively. The decrease of contact angles implies that after the coating layer was applied, the separator has a better wettability compared to the bare Celgard 2325. For greater quantitative testing, the electrolyte uptake and retention amounts were measured.

The electrolyte uptake and retention capacities of the different separators are presented in Table 2. For Celgard 2325 the electrolyte uptake increases from 32 to77 and

252 % for 3, 24 and 144 hours, respectively. This represents the percentage of electrolyte that the separator is able to adsorb. The observed enhancement corresponds to the continuous filling of the porous structure as the immersion time increases.

The same behaviour is observed for the modified separators, although the uptake capacity is much higher than in the Celgard 2325. In the case of MMT/PANI_12/88 the enhancement goes from 168 to 370 % after 3 and 144 hours respectively, meanwhile for MMT/PANI_87/13 the electrolyte uptake capacity changes from 137 to 247 % in the same time interval. For the samples immersed 3 hours in the electrolyte, the highest uptake is observed in the MMT/PANI_12/88 modified separator , this means that this composite absorbs more quickly the electrolyte, probably due to its more open structure and its higher surface area as was seen in the SEM images (Fig. 6 a). Furthermore, the uptake after 144 hours is around 250 % for the unmodified separator and MMT/PANI_87/13 (similar to another MMT based membrane, [40]) while it is 370 % for MMT/PANI_12/88. This is an evidence that MMT/PANI_12/88 modified separator not only has a faster electrolyte uptake but also a higher electrolyte uptake capacity and PANI is responsible for these characteristics. It is worth mentioning that PANI constitutes a hydrogen-bonding matrix contributing to the interaction with the polar organic solvent. Conversely, the PP layer in the bare Celgard is hydrophobic resulting in poor wettability. The three-dimensional and multilayered network structure and the high specific surface area of the composites can absorb more liquid electrolyte and enhance the ion conductivity of LIB, as further discussed below [16].

The electrolyte retention capacity is assigned to the percentage of electrolyte in the total mass of the wetted separator. For all samples, it reaches a value between 70 to 80% after 144 hours. However, at shorter times Celgard 2325 has only 24%, meanwhile, for the modified separators this value is around 60%. Similar results were obtained in ref [41], showing that the addition of PANI in a polymeric membrane further increase the electrolyte uptake and retention capability due to an enhancement of the porous structure and to the great affinity of PANI towards this kind of electrolytes. Nevertheless, the higher absorption of liquid electrolytes may result in a loss of mechanical strength so the combination of PANI with MMT is a promising choice to both increase the electrolyte affinity and also keep the mechanical strength of the separator.

Ionic conductivity of the separator is the most critical factor to achieve good electrochemical performance in LIBs. Figure 7 shows the ionic conductivity dependence on temperatures of the bare and coated Celgard 2325, between 25 and 65 °C. The ionic

conductivities were calculated from the impedance measured at each temperature; the bulk resistance is the intercept with the real axis at high frequencies. The EIS results are shown in Figure SI 4. The results obtained for the modified separators are higher at all temperatures and similar among them.

Table 2 displays the ionic conductivity results obtained from impedance spectroscopy at OCP (open circuit potential), measuring the EIS in 6 hours time interval (EIS spectra are shown in Figure SI 4). The ionic conductivity of Celgard 2325 (0.20 mS cm^{-1}) is much lower than the ones obtained for the coated separators (within 4.22 and 4.29 mS cm^{-1}). Ye et al., 2015 [42] proposed three factors that contribute to the ionic conductivity in PANI membranes: the membrane porosity; the presence of nanochannels in their structure, and the lone pair electrons on nitrogen atoms of PANI that could form electron donator-receptor complexes with Li ions. In the MMT/PANI composites, we are not able to confirm the presence of nanochannels from SEM images, although there is a great porosity in both samples. Besides, very similar values of ionic conductivity were obtained for both modified separators suggesting that the PANI fraction does not play a key role in ionic conductivity. In summary, the most important factor is the presence of inner porosity that allows the uptake of a huge amount of electrolyte. It is worth noting that at 3 hours the electrolyte uptake capacity is very similar among the two coated separator which is five times larger than that of bare Celgard.

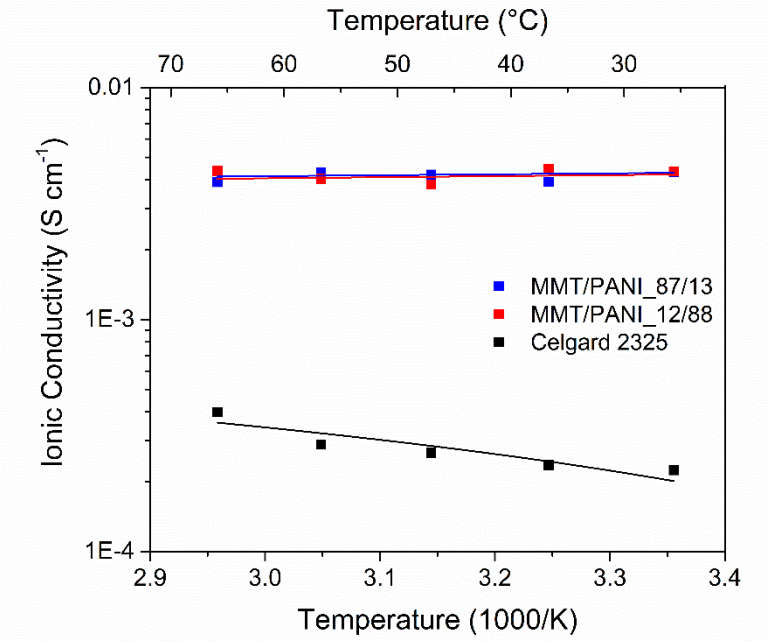

Figure 7. Ionic conductivity vs. temperature for bare and coated Celgard separators. Lines correspond to linear fitting of results.

Concerning electronic conductivity (Table 2), an increase can be seen when a higher percentage of conducting polymer is present in the composite. The obtained values well agree with the values in the literature [12,20,26]. This behaviour can be attributed to alterations in the structure of intra-chain and inter-chain of polymer arrangements produced by the presence of the clay. For the sample with a high amount of clay (MMT/PANI_87/13), conductive polymeric islands are isolated one from the other, breaking the inter-chain connections. On the other hand, when the amount of PANI increases a 're-connection' of conducting polymeric islands takes place increasing the bulk conductivity. Additionally, MMT layers can also affect the intra-chain PANI arrangements influencing the delocalization and the nature of charge carriers in the polymer [19].

Table 2. Capacity of the separators to uptake (φ), to retain (ρ) the liquid electrolyte, ionic and electronic conductivity.

Sample	**φ (%)**			**ρ (%)**			**Ionic Conductivity (Scm^{-1}) at 25°C**	**Electronic Conductivity (Scm^{-1})**
	3 hs	**24 hs**	**144 hs**	**3 hs**	**24 hs**	**144 hs**		
Celgard 2325	32	77	252	24	44	72	$2.0.10^{-4}$	-
MMT/PANI_12/88	168	252	370	63	72	79	$4.3.10^{-3}$	3.10^{-3}
MMT/PANI_87/13	137	129	247	58	56	71	$4.2.10^{-3}$	4.10^{-4}

3.3 Electrochemical performance of assembled cells

The spinel $LiNi_{0.5}Mn_{1.5}O_4$ is a promising high-voltage cathode material for the development of high-energy Li-ion batteries. The major drawback of this material is the disproportionation reaction of Mn^{3+} to Mn^{2+}, which is soluble into the electrolyte, and moves towards the anode where it catalyses undesired reactions that cause a capacity fade in the battery.

The cells with Celgard 2325 and the MMT/PANI coated separators were cycled 10 times at C/10 and then 200 times at C/5. Figure 8 shows the cycling performance and the coulombic efficiency, the first cycle at C/5 and after 150 cycles.

At the first cycle (C/10), the charge-discharge galvanostatic response is similar in the three cells, meanwhile, after 150 cycles, the ΔE is smaller for MMT/PANI_87/13 than the other samples. In addition, a lower capacity fade is observed for what locate this composite as a promising material to be used in Li ion batteries. The capacity fade was calculated considering the specific capacity at the 1st cycle and the one at the 200th cycle. It is corroborated that the capacity fade for MMT/PANI_12/88 (80%) is lower than that for MMT/PANI_87/13 (53%), meanwhile for the Celgard without the membrane is 62%. It is worth noting that all the samples show coulombic efficiencies higher than 96%, pointing out good reversibility of lithium ion (de)-intercalation [43].

Although both modified separators have similar ionic conductivities, better electrochemical performances are obtained for MMT/PANI_87/13 coating, suggesting that other factors contribute to the cyclability. Similar behaviours were found in the literature. For example, Yang et al., 2017 [16] reported that the presence of MMT in the membrane is effective to suppress $LiPF_6$ decomposition and reduce the contents of F^- and therefore the Mn^{3+} disproportion and further migration of Mn^{2+} to the anode. Feng et al., 2018 [44] indicated that silica aerogel modified separators with large specific surface area can absorb the impurity acids produced by the electrolyte during the cycling process and contribute to its cyclability. Furthermore, MMT could retain Mn^{2+} by electrostatic interaction with the negative siloxane layers avoiding its migration to the anode. Also, the presence of MMT in the coating layer could affect the lithium ion migration rate, by reducing the steric hindrance of solvated Li^+ [45,46]. Post-mortem studies are being performed to identify these mechanisms. In conclusion, the composition of the coating layer contributes mostly to the improvement in the electrochemical performance.

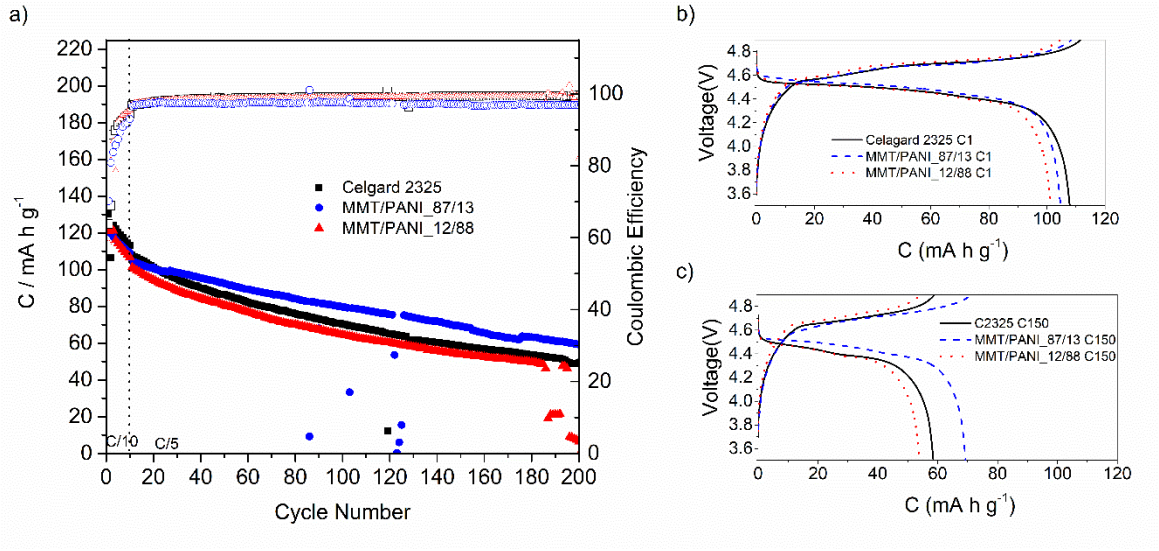

Figure 8. Cycling performance (filled symbols) and coulombic efficiency (empty symbols) of LMNO vs. graphite cell using bare and coated Celgard separators (a). Galvanostatic response for first cycle (b) and cycle 150 (c) at C/5.

4. Conclusions

Two MMT/PANI composites were successfully synthesised from polyaniline and natural MMT. The mass ratios used were adequate to obtain two different structural arrangements, leading to composites with different compositions, properties and behaviours.

Thermogravimetric analyses allowed to determine the percentage of polymer and clay in each composite. Furthermore, this technique showed that MMT conferred thermal resistance to the composites. The presence of PANI inside the interlaminar space of MMT was verified in both composites by XRD analyses. From FTIR analysis the presence of PANI in its conductive form (emeraldine salt) was verified. Zeta potential measurements indicated that PANI was preferentially located in between the clay slabs in MMT/PANI_87/13, while for MMT/PANI_12/88, the presence of emeraldine-PANI in the exposed surface was evidenced. XPS allowed determining the Si/N ratio that agreed with the TG results.

After all the exhaustive characterization it was possible to propose a structural compositional model for the two different composites. MMT/PANI_12/88 consists of clay slabs immersed in a polymeric matrix, meanwhile MMT/PANI_87/13 is an intercalated composite where PANI is preferentially located in the interlamellar spaces of MMT.

These composites were used to modify a commercial separator (Celgard 2325), typically used in lithium ion batteries. Through SEM images, the characteristic morphologies of each composite in the applied layer were observed. This modification enhanced the porosity, electrolyte uptake and retention capacities and ionic conductivity of the separator.

Finally, the modified separators were used to assemble full cells (graphite vs. LNMO). The cell with the MMT/PANI_87/13 modified separator showed the best cycling performance, since it presented a better retention capacity than the cell with the unmodified separator. In addition, it presented a lower ΔE between charge and discharge plateaus. From these preliminary electrochemical studies, we conclude that the composite MMT/PANI_87/13 is a promising material to be used in ion lithium batteries.

Acknowledgements:

Authors gratefully acknowledge for financial support provided by e-CAIMAN project (G.A. 653331, H2020 E.U. 3.4, and POLAR project (Call for Joint Projects for the internationalization of Research, Politecnico di Torino). The authors thank Dra. Rosa M. Torres Sanchez from CETMIC for providing MMT sample.

References

[1] A.F. Shestakov, O.E. Romanyuk, A. V. Mumyatov, S.Y. Luchkin, A.A. Slesarenko, O. V. Yarmolenko, K.J. Stevenson, P.A. Troshin, Theoretical and experimental evidence for irreversible lithiation of the conformationally flexible polyimide: Impact on battery performance, J. Electroanal. Chem. 836 (2019) 143–148. https://doi.org/10.1016/j.jelechem.2019.01.063.

[2] C.M. Costa, E. Lizundia, S. Lanceros-Méndez, Polymers for advanced lithium-ion batteries: State of the art and future needs on polymers for the different battery components, Prog. Energy Combust. Sci. 79 (2020). https://doi.org/10.1016/j.pecs.2020.100846.

[3] X. Hong, Y. Liu, Y. Li, X. Wang, J. Fu, X. Wang, Application progress of polyaniline, polypyrrole and polythiophene in lithium-sulfur batteries, Polymers (Basel). 12 (2020). https://doi.org/10.3390/polym12020331.

[4] G. Ma, Z. Wen, Q. Wang, C. Shen, P. Peng, J. Jin, X. Wu, Enhanced performance of lithium sulfur battery with self-assembly polypyrrole nanotube film as the functional interlayer, J. Power Sources. 273 (2015) 511–516. https://doi.org/10.1016/j.jpowsour.2014.09.141.

[5] Y. Luo, R. Guo, T. Li, F. Li, Z. Liu, M. Zheng, B. Wang, Z. Yang, H. Luo, Y. Wan, Application of Polyaniline for Li-Ion Batteries, Lithium–Sulfur Batteries, and Supercapacitors, ChemSusChem. 12 (2019) 1591–1611. https://doi.org/10.1002/cssc.201802186.

[6] N. Harfouche, B. Nessark, F.X. Perrin, Electrochemical and surface characterization of composite material: Polyaniline/LiMn2O4, J. Electroanal. Chem. 756 (2015) 179–185. https://doi.org/10.1016/j.jelechem.2015.08.031.
[7] Y. Dong, Y. Ding, Y. Zhou, J. Chen, C. Wang, Differential pulse anodic stripping voltammetric determination of Pb ion at a montmorillonites/polyaniline nanocomposite modified glassy carbon electrode, J. Electroanal. Chem. 717–718 (2014) 206–212. https://doi.org/10.1016/j.jelechem.2014.01.014.
[8] C.H. Chang, S.H. Chung, A. Manthiram, Ultra-lightweight PANiNF/MWCNT-functionalized separators with synergistic suppression of polysulfide migration for Li-S batteries with pure sulfur cathodes, J. Mater. Chem. A. 3 (2015) 18829–18834. https://doi.org/10.1039/c5ta05053g.
[9] A. Kenane, A.C. Galca, E. Matei, A. Yahyaoui, A. Hachemaoui, A.M. Benkouider, C. Bartha, M.C. Istrate, M. Galatanu, O. Rasoga, A. Stanculescu, Synthesis and characterization of conducting aniline and o-anisidine nanocomposites based on montmorillonite modified clay, Appl. Clay Sci. 184 (2020) 105395. https://doi.org/10.1016/j.clay.2019.105395.
[10] M.G. Hosseini, M. Jafari, R. Najjar, Effect of polyaniline-montmorillonite nanocomposite powders addition on corrosion performance of epoxy coatings on Al 5000, Surf. Coatings Technol. 206 (2011) 280–286. https://doi.org/10.1016/j.surfcoat.2011.07.012.
[11] J. Chen, X. Hong, Y. Zhao, Y. Xia, D. Li, Q. Zhang, Preparation of flake-like polyaniline/montmorillonite nanocomposites and their application for removal of Cr(VI) ions in aqueous solution, J. Mater. Sci. 48 (2013) 7708–7717. https://doi.org/10.1007/s10853-013-7591-3.
[12] L. Kulhánková, J. Tokarský, V. Matějka, P. Peikertová, S. Vallová, K. Mamulová Kutláková, V. Stýskala, P. Čapková, Electrically conductive and optically transparent polyaniline/ montmorillonite nanocomposite thin films, Thin Solid Films. 562 (2014) 319–325. https://doi.org/10.1016/j.tsf.2014.05.006.
[13] H. Zhang, X. Wang, Y. Liang, Preparation and characterization of a Lithium-ion battery separator from cellulose nanofibers, Heliyon. 1 (2015) 1–16. https://doi.org/10.1016/j.heliyon.2015.e00032.
[14] C. Shi, J. Dai, C. Li, X. Shen, L. Peng, P. Zhang, D. Wu, D. Sun, J. Zhao, A modified ceramic-coating separator with high-temperature stability for lithium-ion battery, Polymers (Basel). 9 (2017) 10–14. https://doi.org/10.3390/polym9050159.
[15] L. Yu, J. Miao, Y. Jin, J.Y.S. Lin, A comparative study on polypropylene separators coated with different inorganic materials for lithium-ion batteries, Front. Chem. Sci. Eng. 11 (2017) 346–352. https://doi.org/10.1007/s11705-017-1648-9.
[16] S. Yang, H. Qin, X. Li, H. Li, P. Yao, Enhancement of Thermal Stability and Cycling Performance of Lithium-Ion Battery at High Temperature by Nano-ppy/OMMT-Coated Separator, J. Nanomater. 2017 (2017). https://doi.org/10.1155/2017/6948183.
[17] A.P. Magnoli, L. Tallone, C.A.R. Rosa, A.M. Dalcero, S.M. Chiacchiera, R.M. Torres Sanchez, Commercial bentonites as detoxifier of broiler feed contaminated with aflatoxin, Appl. Clay Sci. 40 (2008) 63–71. https://doi.org/10.1016/j.clay.2007.07.007.
[18] F. Yarza, C.F. Morantes, M.L. Montes, N. Bellotti, J. Salduondo, S. Yapar, F. Cravero, R.M. Torres Sánchez, Quantification of the distribution of cetylpyridinium chloride on the external and internal surfaces of montmorillonite: Relevance in antifungal activity assessment, Mater. Chem. Phys. 253 (2020) 123390. https://doi.org/10.1016/j.matchemphys.2020.123390.
[19] G.M. do Nascimento, V.R.L. Constantino, R. Landers, M.L.A. Temperini,

Spectroscopic characterization of polyaniline formed in the presence of montmorillonite clay, Polymer (Guildf). 47 (2006) 6131–6139. https://doi.org/10.1016/j.polymer.2006.06.036.
[20] J.A. Marins, B.G. Soares, A facile and inexpensive method for the preparation of conducting polyaniline-clay composite nanofibers, Synth. Met. 162 (2012) 2087–2094. https://doi.org/10.1016/j.synthmet.2012.10.015.
[21] F.D. Zailan, R.S. Chen, D. Shahdan, S. Ahmad, Effect of conductive polyaniline in thermoplastic natural rubber blends on the mechanical, thermal stability, and electrical conductivity properties, J. Appl. Polym. Sci. 136 (2019) 1–9. https://doi.org/10.1002/app.47527.
[22] S. Yariv, Differential Thermal Analysis (DTA) in the Study of Thermal Reactions of Organo-Clay Complexes, Nat. Lab. Therm. Geochemical Process. (2003) 253–296. https://doi.org/10.1007/978-94-017-0111-2_8.
[23] Y. Hattab, N. Benharrats, Electrical and thermal properties of PANI–Mmt nanocomposites in strongly acidic aqueous media, SN Appl. Sci. 1 (2019). https://doi.org/10.1007/s42452-019-0703-1.
[24] Q. Zhou, R.L. Frost, H. He, Y. Xi, Changes in the surfaces of adsorbed para-nitrophenol on HDTMA organoclay-The XRD and TG study, J. Colloid Interface Sci. 307 (2007) 50–55. https://doi.org/10.1016/j.jcis.2006.11.016.
[25] D. Lee, K. Char, Thermal degradation behavior of polyaniline in polyaniline/Na+-montmorillonite nanocomposites, Polym. Degrad. Stab. 75 (2002) 555–560. https://doi.org/10.1016/S0141-3910(01)00259-2.
[26] S. Yoshimoto, F. Ohashi, T. Kameyama, Simple preparation of sulfate anion-doped polyaniline-clay nanocomposites by an environmentally friendly mechanochemical synthesis route, Macromol. Rapid Commun. 25 (2004) 1687–1691. https://doi.org/10.1002/marc.200400299.
[27] K. Emmerich, M. Plötze, G. Kahr, Reversible collapse and Mg2+ release of de- and rehydroxylated homoionic cis-vacant montmorillonites, Appl. Clay Sci. 19 (2001) 143–154. https://doi.org/10.1016/S0169-1317(01)00049-7.
[28] F. Farshi Azhar, A. Olad, A. Mirmohseni, Development of novel hybrid nanocomposites based on natural biodegradable polymer-montmorillonite/polyaniline: Preparation and characterization, Polym. Bull. 71 (2014) 1591–1610. https://doi.org/10.1007/s00289-014-1143-0.
[29] I. Bekri-Abbes, E. Srasra, Characterization and AC conductivity of polyaniline-montmorillonite nanocomposites synthesized by mechanical/chemical reaction, React. Funct. Polym. 70 (2010) 11–18. https://doi.org/10.1016/j.reactfunctpolym.2009.09.008.
[30] F. Thomas, L.J. Michot, D. Vantelon, E. Montargès, B. Prélot, M. Cruchaudet, J.F. Delon, Layer charge and electrophoretic mobility of smectites, Colloids Surfaces A Physicochem. Eng. Asp. 159 (1999) 351–358. https://doi.org/10.1016/S0927-7757(99)00291-5.
[31] W.A. Marmisollé, M.I. Florit, D. Posadas, Acid-base equilibrium in conducting polymers. The case of reduced polyaniline, J. Electroanal. Chem. 734 (2014) 10–17. https://doi.org/10.1016/j.jelechem.2014.03.003.
[32] W. Lyu, M. Yu, J. Feng, W. Yan, Highly crystalline polyaniline nanofibers coating with low-cost biomass for easy separation and high efficient removal of anionic dye ARG from aqueous solution, Appl. Surf. Sci. 458 (2018) 413–424. https://doi.org/10.1016/j.apsusc.2018.07.074.
[33] H. Seyama, M. Soma, Bonding-state characterization of the constitutent elements of silicate minerals by X-ray photoelectron spectroscopy, J. Chem. Soc. Faraday Trans. 1 Phys. Chem. Condens. Phases. 81 (1985) 485–495.

https://doi.org/10.1039/F19858100485.
[34] A.G. Ginder, J. M., Epstein, A. J., & MacDiarmid, ELECTRONIC PHENOMENA IN POLYANILINE, Synth. Met. 29 (1989) 395–400. https://www.unhcr.org/publications/manuals/4d9352319/unhcr-protection-training-manual-european-border-entry-officials-2-legal.html?query=excom 1989.
[35] U. Fano, Effects of configuration interaction on intensities and phase shifts, Phys. Rev. 124 (1961) 1866–1878. https://doi.org/10.1103/PhysRev.124.1866.
[36] M. Dirican, M. Yanilmaz, A.M. Asiri, X. Zhang, Polyaniline/MnO2/porous carbon nanofiber electrodes for supercapacitors, J. Electroanal. Chem. 861 (2020). https://doi.org/10.1016/j.jelechem.2020.113995.
[37] B. Kim, J. Jung, S. Hong, J. Joo, A.J. Epstein, J.W. Kim, H.J. Choi, Nanocomposite of Polyaniline and Na + - Montmorillonite Clay, (2002) 1419–1423.
[38] G.M. do Nascimento, N.A. Pradie, Deprotonation , Raman dispersion and thermal behavior of polyaniline – montmorillonite nanocomposites, Synth. Met. 217 (2016) 109–116. https://doi.org/10.1016/j.synthmet.2016.03.016.
[39] Z. Zhang, Y. Han, T. Li, T. Wang, X. Gao, Q. Liang, L. Chen, Polyaniline / montmorillonite nanocomposites as an effective fl ame retardant and smoke suppressant for polystyrene, Synth. Met. 221 (2016) 28–38. https://doi.org/10.1016/j.synthmet.2016.10.009.
[40] M. Raja, T.P. Kumar, G. Sanjeev, L. Zolin, C. Gerbaldi, A.M. Stephan, Montmorillonite-based ceramic membranes as novel lithium-ion battery separators, Ionics (Kiel). 20 (2014) 943–948. https://doi.org/10.1007/s11581-013-1030-y.
[41] U.R. Farooqui, A.L. Ahmad, N.A. Hamid, Effect of polyaniline (PANI) on Poly(vinylidene fluoride-co-hexaflouro propylene) (PVDF-co-HFP) polymer electrolyte membrane prepared by breath figure method, Polym. Test. 60 (2017) 124–131. https://doi.org/10.1016/j.polymertesting.2017.03.012.
[42] W. Ye, J. Zhu, X. Liao, S. Jiang, Y. Li, H. Fang, H. Hou, Hierarchical three-dimensional micro/nano-architecture of polyaniline nanowires wrapped-on polyimide nanofibers for high performance lithium-ion battery separators, J. Power Sources. 299 (2015) 417–424. https://doi.org/10.1016/j.jpowsour.2015.09.037.
[43] Y. Ma, L.B. Li, G.X. Gao, X.Y. Yang, Y. You, Effect of montmorillonite on the ionic conductivity and electrochemical properties of a composite solid polymer electrolyte based on polyvinylidenedi fl uoride / polyvinyl alcohol matrix for lithium ion batteries, Electrochim. Acta. 187 (2016) 535–542.
[44] G. Feng, Z. Li, L. Mi, J. Zheng, X. Feng, W. Chen, Polypropylene / hydrophobic-silica-aerogel-composite separator induced enhanced safety and low polarization for lithium-ion batteries, J. Power Sources. 376 (2018) 177–183. https://doi.org/10.1016/j.jpowsour.2017.11.086.
[45] C. Xue, D. Jin, H. Nan, H. Wei, H. Chen, S. Xu, A novel polymer-modified separator for high-performance lithium-ion batteries, J. Power Sources. 449 (2020) 227548. https://doi.org/10.1016/j.jpowsour.2019.227548.
[46] R. Zahn, M.F. Lagadec, M. Hess, V. Wood, Improving Ionic Conductivity and Lithium-Ion Transference Number in Lithium-Ion Battery Separators, (2016) 6–11. https://doi.org/10.1021/acsami.6b12085.